JOURNAL OF MATERIALS SCIENCE 32 (1997) 2835–2848

Processing, microstructure and fracture behaviour of a spray atomized and deposited aluminium–silicon alloy

S. ANAND, T. S. SRIVATSAN
Department of Mechanical Engineering, The University of Akron, Akron, OH 44325-3903 USA
YUE WU, E. J. LAVERNIA
Department of Chemical Engineering and Materials Science, University of California, Irvine, CA 92717 USA

In this study a hypereutectic aluminium–silicon alloy was synthesized by spray atomization and deposition technique. Microstructure characterization studies were performed to provide an understanding of the influence of spray processing on microstructure of the hypereutectic alloy. Ambient and elevated temperature tensile tests reveal the spray-processed alloy to have better strength and ductility than a conventional ingot metallurgy processed alloy having the same chemical composition. The quasi-static fracture characteristics of the spray-processed alloy is presented and discussed in light of processing and intrinsic microstructural effects.

1. Introduction

The intrinsically good wear resistance characteristics coupled with low coefficient of thermal expansion (CTE) has provided the necessary impetus in considering the family of aluminium–silicon alloys as potentially viable candidates for a spectrum of applications spanning the automotive, aerospace and electrical industries [1–3]. Recent efforts to engineer enhanced physical and mechanical properties have focused on compositional modifications as an affordable and promising approach for improving the strength, ductility (to include fabricability) and the fracture-related properties of these alloys. This development culminated in hypereutectic compositions. The salient features of the family of hypereutectic aluminium–silicon alloys is their low CTE coupled with excellent wear resistance characteristics. The outstanding wear resistance characteristic arises because of a high volume fraction of the primary silicon phase.

Besides conventional ingot metallurgy (IM) processing an attractive and viable processing technique to synthesize the family of hypereutectic aluminium–silicon alloys is rapid solidification (RS) processing. Extensive use of IM processing was restricted by the range of alloy compositions. This can be attributed to the formation and presence of coarse primary silicon phase and eutectic phases. These phases result as a direct consequence of the low solidification rate that is typical of IM processing. The presence of coarse primary silicon phase and other eutectic phases can be obviated through the use of modifying elements or refining agents such as sodium, sulphur and strontium. In the absence of refining elements, the primary silicon phase dispersoids are relatively coarse, of the order 30–100 μm in diameter. The presence of a distribution of coarse particulates of silicon in the alloy matrix is directly responsible for the inferior ductility and limited workability of the family of IM processed hypereutectic Al–Si alloys [4]. Many of the problems associated with conventional IM processing can be effectively overcome by the use of rapid solidification processing such as melt spinning [5], atomization [1, 3] and spray deposition [6]. The most significant benefit with the use of RS processing is a substantial modification of the size, morphology and distribution of the primary silicon phase, in the alloy matrix, relative to that present in the conventionally processed counterpart.

The performance of the family of hypereutectic aluminium–silicon alloys is largely governed by the competing and mutually interactive influences of: (a) the size and distribution of the primary silicon phase, (b) nature of cohesion between the matrix and the silicon phase, and (c) fracture characteristics of the silicon particulates [7]. Attempts to increase nucleation frequency, while concurrently minimizing coarsening of the primary silicon during solidification, can be achieved either through controlled alloying additions [8, 9], or by using RS processing to enhance nucleation frequency with a resultant decrease in the coarsening kinetics [6, 9].

The objective of this study was to provide an insight into the microstructure, tensile properties and fracture behaviour of a spray-atomized and deposition processed, henceforth referred to in this paper as the spray-processed, hypereutectic aluminium–silicon

0022–2461

alloy. The tensile properties of the spray-processed alloy is compared with a conventional IM processed alloy having identical chemical composition. The quasi-static fracture characteristics of the alloy is compared and discussed in light of processing and intrinsic microstructural effects.

2. Spray atomization and deposition processing

High deposition rate spray forming has during the last decade emerged as a potentially viable technology to effectively reduce production costs, while concurrently improving the workability and mechanical properties of a spectrum of metallic systems and their composite counterparts [10–15]. The technique of spray deposition processing is essentially a two-step process route that involves [11, 13, 15–17]:

(a) An energetic disintegration of the molten metal, by inert gas, into micron-sized droplets (atomization).

(b) The subsequent deposition of the mixture of solid, liquid and partially solidified droplets on a substrate surface (deposition).

The droplets eventually collect as a coherent preform, the microstructure of which is largely dictated by the solidification conditions of the droplets during impact. This synthesis methodology offers a potentially attractive manufacturing route for the following reasons:

1. The highly efficient heat extraction during atomization ensures the maintenance of relatively low processing temperatures which limits large scale segregation and associated coarsening phenomena.
2. The inert conditions required for atomization and deposition minimize surface oxidation and other deleterious surface reactions.
3. Spray atomization and deposition can potentially be used for near net-shape manufacturing of difficult to form materials, such as the ordered intermetallic compounds and discontinuously-reinforced metal–matrix composites [15, 17–19].

A detailed study of the solidification mechanisms that govern the evolution of microstructure during spray atomization and deposition is rendered complex by the extreme differences in thermal environment both before and after impact of the droplets with the deposition surface. During atomization, the violent and/or rapid extraction of thermal energy by the atomization gas promotes the formation of highly refined microstructures [20]. In contrast, the solidification conditions after the distribution of droplets strikes or arrives at the deposition surface are governed by relatively sluggish cooling rates [21, 22]. The microstructure of spray-atomized and -deposited materials is generally reported to exhibit spheroidal or "equiaxed" grains, a feature that is consistently observed regardless of alloy composition [23–25]. A comprehensive study of the phenomena has been reported and discussed in detail elsewhere [25]. Furthermore, recent work on the interfacial behaviour in metal–matrix composites processed by spray atomization and deposition has provided some interesting insights into the thermal and solidification conditions that govern microstructural evolution [26–29]. In fact, spray atomization and deposition processing exhibits the beneficial characteristics of powder metallurgy (PM) processing without the numerous processing concerns, that is, powder production, storage and handling, sintering and hot consolidation.

3. Materials

The starting material used in this study was commercial quality cast aluminium alloy A390 provided by Reynolds Metals Company (Richmond, VA) in the form of ingot bars. The nominal chemical composition (in weight percent) of the as-received material is Al–17Si–4.5Cu–0.6Mg.

Samples of the rapidly solidified (RS) hypereutectic alloy, of identical composition to the cast IM counterpart A390, were prepared by utilizing a spray atomization and deposition approach, henceforth referred to in this manuscript as spray-processed AS17. The synthesis involves the following procedure:

1. The as-received A390 alloy was superheated to a temperature of 1073 K in a graphite crucible in an environment of nitrogen (N_2) gas at 1.013×10^5 Pa. To avoid oxidation of the hypereutectic aluminium–silicon alloy during spray deposition processing, the experiments were conducted inside an environmental chamber which was evacuated down to a pressure of 200 Pa and back-filled with nitrogen.
2. The superheated alloy was delivered to an atomizer through a ceramic delivery tube, where it was disintegrated into a fine dispersion of micron-sized droplets using nitrogen gas and at an atomization pressure of 3.1 MPa.
3. Following atomization, the partially solidified droplets were collected on a hydraulically controlled, water-cooled, rotating copper substrate, positioned at a distance of 46 cm from the atomizer nozzle. The droplets eventually collect as a coherent preform.

The spray atomization and deposition apparatus used in this study is shown in Fig. 1. A succinct summary of the primary processing parameters used in this study is provided in Table I. The selection of the atomizer–substrate distance and the processing parameters

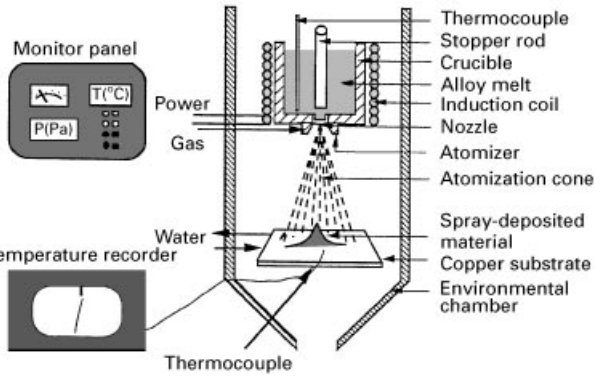

Figure 1 Schematic diagram showing experimental apparatus used for spray atomization and deposition processing.

TABLE I Primary processing parameters

Atomization gas	Nitrogen
Atomization pressure	3.1 MPa
Atomized droplet flight distance	46 cm
Pouring temperature	1073 K
Ratio of metal/gas mass flow rates	1.3

used was made after a numerical and experimental study, details of which can be found elsewhere [15].

The as-spray deposited alloy was sectioned into billets of size 2.54 cm diameter × 8 cm length. The billets were hot extruded at 773 K using an extrusion ratio of 16 : 1. The purpose of extruding at an elevated temperature was to close the micrometre-sized pores quite typical of spray-atomized and -deposited materials [6, 30, 31]. The extruded bar was allowed to cool in ambient air.

4. Experimental procedure

4.1. Microstructure

The initial microstructure of the spray processed (AS17) alloy and the conventional IM processed (sand cast + extruded A390) counterpart was characterized by optical microscopy after specimen preparation by standard metallography and polishing techniques. The samples were etched with Keller's reagent and examined in an optical microscope and photographed using a standard bright-field illumination technique to reveal: (i) the grain boundaries, (ii) second-phase morphology and distribution, and (iii) overall grain morphology. The primary and other secondary phases present in the microstructure were identified using transmission electron microscopy (TEM), selected area diffraction (SAD), and X-ray diffraction. The TEM studies were conducted using a Phillips CM20 transmission electron microscope operated at an accelerating voltage of 200 keV. The X-ray diffraction experiments were performed on a Siemens D5000 diffractometer using CuK_α radiation. For phase identification, X-ray diffraction patterns were obtained in the diffraction angle (2θ) range between 20 and 90 degree. The supersaturation of alloying elements was determined using X-ray lattice parameter measurements. To that effect, the high-angle diffraction peaks of aluminium (4 0 0), (3 3 1) and (4 2 2) were used to determine the lattice parameter.

4.2. Mechanical testing

Tensile test samples, conforming to specifications in ASTM standard E-8-93, were precision machined from both the spray-processed (AS17) and IM-processed alloys. Uniaxial tensile tests were performed up to failure on a fully automated, closed-loop, servohydraulic mechanical test machine (Instron) equipped with a 100 kN load cell. The specimens were deformed at a constant strain rate of $10^{-4}\,s^{-1}$. The tests were performed in controlled laboratory air environment (relative humidity = 55%) at ambient (30 °C), and elevated temperatures (150 °C). The highest test temperature corresponds to the temperature at which the alloy was artificially aged. The elevated temperature tests were conducted using an Instron environmental chamber (Model 3111). The temperature was controlled with the aid of a temperature controller (a thermocouple-controller unit) fixed on the specimen's surface. Maximum temperature variation was well within 2 °C of the set-point temperature (150 °C) over the entire duration of the test. Ambient temperature varied from 30 to 32 °C, with a maximum 2 °C variation during any given test. Before each test, the specimen was maintained at the test temperature for 30 min so as to achieve stability with the environment. The axial strain was measured using an axial 12.7 mm clip-on extensometer fixed, using rubber bands for room-temperature tests and steel springs for the elevated temperature tests, to the gauge section of the test specimen. The stress and strain measurements, parallel to the load line, were recorded on a PC-based data acquisition system.

4.3. Failure – damage analysis

Fracture surfaces of the deformed and failed tensile samples were examined in a scanning electron microscope (SEM) to: (a) determine the macroscopic fracture mode, and (b) characterize the fine-scale topography and microscopic mechanisms governing quasi-static fracture. The distinction between the macroscopic mode and microscopic fracture mechanism is based on the magnification level at which the observations are made. The macroscopic mode refers to the nature of failure (plane strain, plane stress or a combination of both), while the microscopic mechanism relates to the local failure process (microvoid formation, coalescence and nature of cracking). Samples for SEM observation were obtained from the deformed tensile specimens by sectioning parallel to the fracture surface.

5. Results and discussion

5.1. Microstructure

The optical micrographs of the spray processed (AS17) and conventional IM processed A390 alloy counterpart are shown in Figs 2 and 4. The microstructure of the conventionally processed A390-T6 alloy, in the as-cast plus extruded condition, reveals the primary silicon particulates, of varying size, distributed randomly through the alloy matrix (Fig. 2a). The non-uniform size and distribution of the particulates resulted in particulate-rich and particulate depleted regions (Fig. 2b). The particulates were aligned in the direction of extrusion. Besides the presence of block-like silicon particulates, isolated pockets of a eutectic silicon phase, having a flake-like morphology with large aspect ratio, was also evident (Fig. 2c). TEM observations revealed secondary phases decorating the interdendritic boundaries of the α-aluminium phase. These phases were identified by electron diffraction to be Al_2Cu and Al_xCu_yMg (Fig. 3).

Optical microstructure of the spray processed AS17 alloy revealed a near-uniform distribution of

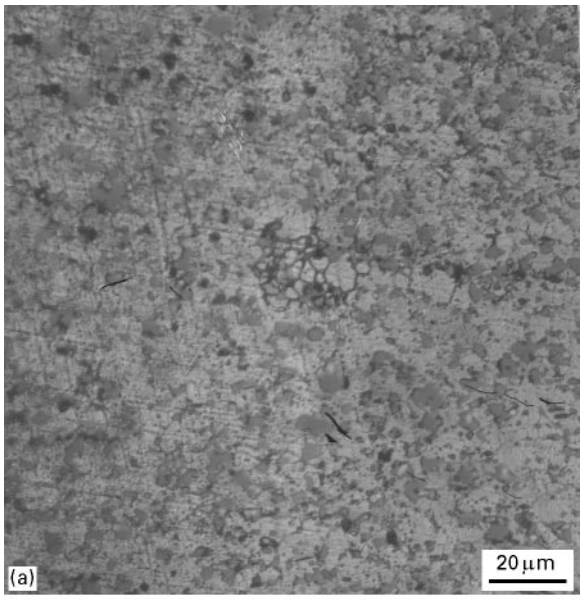

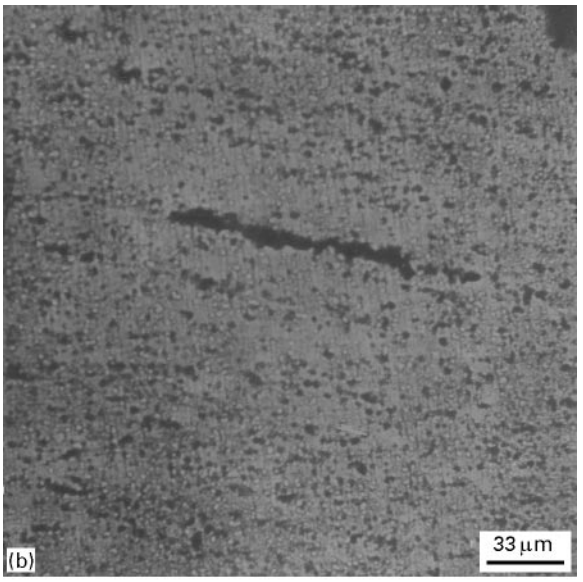

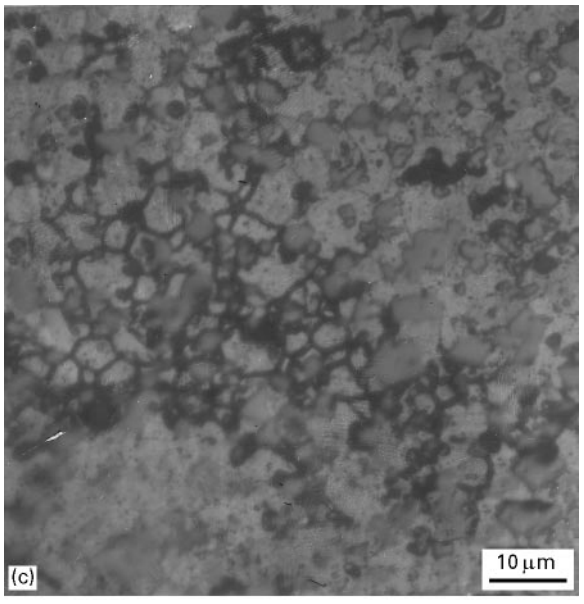

Figure 2 Optical micrographs showing microstructure of the spray-processed (spray atomized and deposited) alloy.

dispersoids (Fig. 4a) and equiaxed shaped grains (Fig. 4c). The presence of eutectic Al–Si phase and coarse primary silicon particulates in the conventionally processed IM counterpart was suppressed. The dispersoids present in the α-aluminium matrix exhibited a faceted particulate morphology (Fig. 4b). The dispersoid particles were identified to be the silicon particulates by the X-ray diffraction spectrum (Fig. 5). The presence of particulate silicon dispersoids has been documented by other investigators working on rapid solidification (RS) processed hypereutectic aluminium–silicon alloys [2, 3, 7, 32]. The particulate silicon dispersoids arise from the high cooling rates of the order of 10^4–10^6 K s^{-1}, typical of rapid solidification processing. The key factors contributing to the formation and presence of the particulate-like silicon phase in the spray deposited material result from the conjoint and mutually interactive influences of:

1. The relativity high cooling rates present during spray deposition (of the order 2×10^3 K s^{-1} to 4×10^3 K s^{-1} [33, 34], which has the intrinsic ability to alter the morphological stability of the silicon phase.

2. Repeated deformation and fracture experienced by the partially solidified droplets during spray deposition has a tendency to break the silicon phase that formed prior to deposition on the substrate. The presence of such silicon phase has a tendency to increase the nucleation kinetics by increasing the number density of nuclei in the top layer of the spray deposited material, thereby effectively suppressing the formation of eutectic aluminium–silicon during deposition.

3. Formation and presence of the particulate-like silicon phase is the end result of a competition between nucleation and growth in front of the solid/liquid interface in the top layer of the spray deposited material. The presence of a concentration gradient in front of the solid/liquid interface causes or promotes the dendritic or planar growth front to be replaced by an equiaxed structure. For the hypereutectic aluminium–silicon alloy, the silicon growth front rejects the aluminium atoms into the liquid alloy. Consequently, there exists a localized region having a low concentration of silicon present in front of the solid–liquid interface. This results in a relatively low liquidus at the interfacial area.

TEM studies revealed the presence of additional secondary phases (Fig. 6). This phase exhibited a spherical morphology. On the basis of selected area diffraction (Fig. 6b) this phase was identified to be Al_2CuMg. This observation accords well with those obtained by Zhou and Duszczyk [35] who reported the presence of Al_2CuMg in copper and magnesium-containing hypereutectic aluminium–silicon alloys.

The presence of near-equiaxed shaped grains (Fig. 4c) conforms well with results obtained by other investigators on both reinforced and unreinforced spray-deposited materials of various compositions [25, 28, 29, 36–39]. The two governing mechanisms

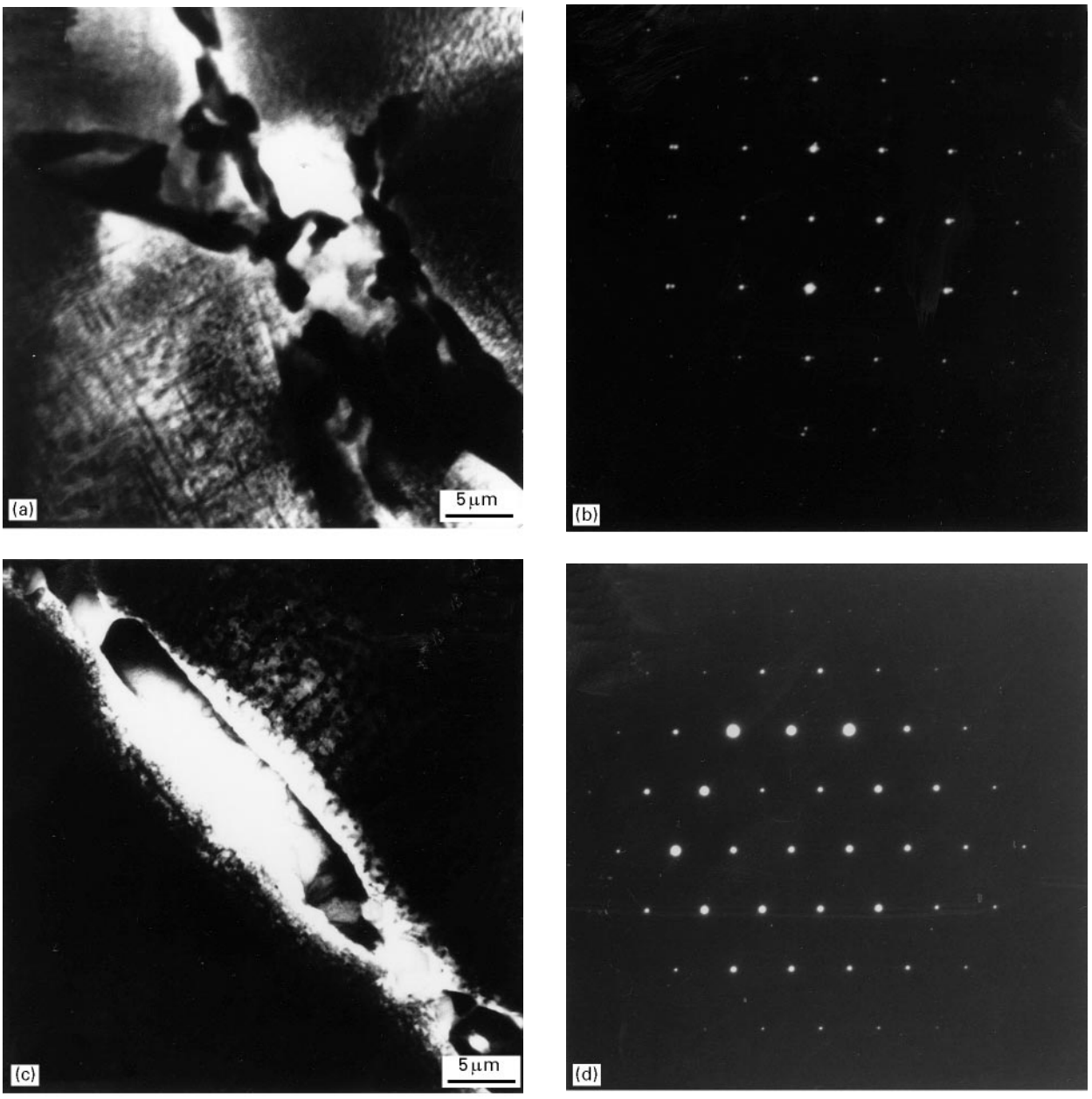

Figure 3 Secondary phases present in the interdendritic regions of the IM A390-T6 alloy: (a) Bright field image of Al_2Cu; (b) Selected area diffraction of the Al_2Cu phase; (c) Bright field image of Al_2CuMg; (d) Selected area diffraction of the Al_2CuMg phase.

that have been proposed to explain the formation of equiaxed grains in spray processed materials are:

1. Equiaxed grain formation by dendrite arm fragmentation [25, 37–39].
2. Equiaxed grain development by the growth and coalescence of the dendrite fragments during solid-state cooling [25].

In the mechanism of dendrite arm fragmentation, the dendrite arm fragments are considered to be the major cause for the formation of equiaxed grains. This occurs as a direct result of the development of a semi-liquid–semi-solid layer on the deposited surface upon the concurrent arrival of the solid, liquid and semi-liquid droplets. Upon impact of the solid and semi-solid droplets with the deposition surface dendrite arm fragments are produced. These fragments act as potential sites for the nucleation of equiaxed grains [37–39].

In the mechanism of solid state cooling, the equiaxed grains evolve from two distinct yet mutually competitive processes [25]:

1. The homogenization of the dendrite arms that did not deform extensively during deposition.
2. The progressive growth and eventual coalescence of the deformed and fractured dendrite arms.

Considering the low melting temperature of the hypereutectic Al–Si alloy used in this study, the mechanism of dendrite arm fragmentation is most likely responsible for the formation of equiaxed grains. Furthermore, the formation of large silicon particulates from the melt provides the necessary impetus for enhanced nucleation through an epitaxy growth mechanism [40]. Thus, a highly heterogeneous mixture of microstructures arrives on the deposition surface and eventually collects as a highly dense preform. The microstructure of the preform is critically dependent

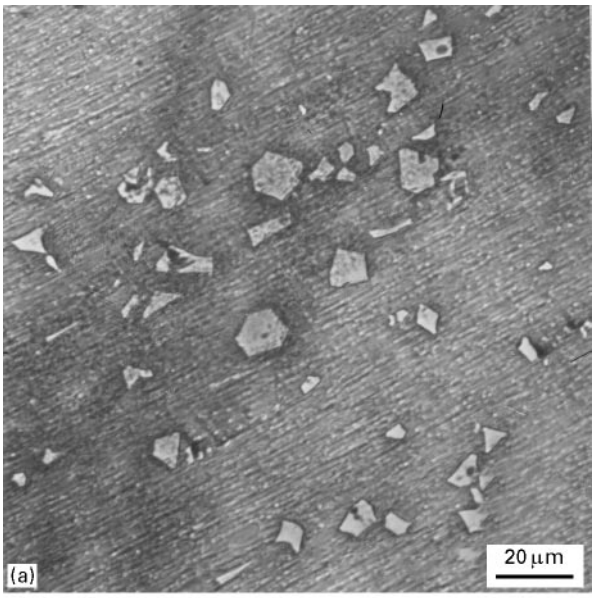

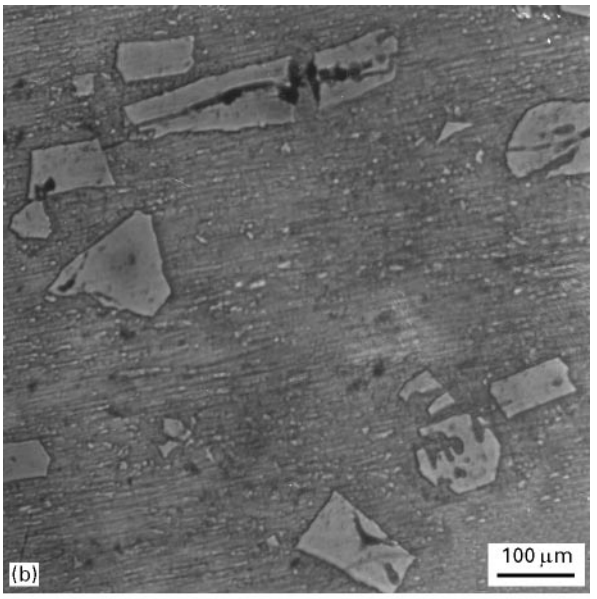

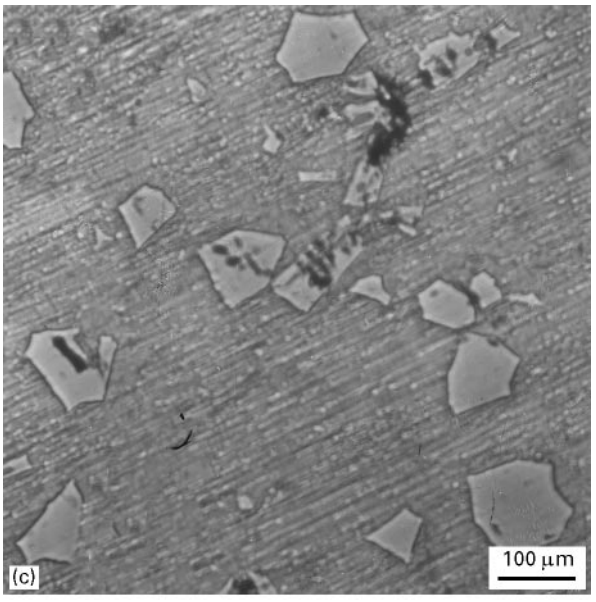

Figure 4 Optical micrographs showing microstructure of the conventionally processed (ingot cast + extruded) A390 alloy.

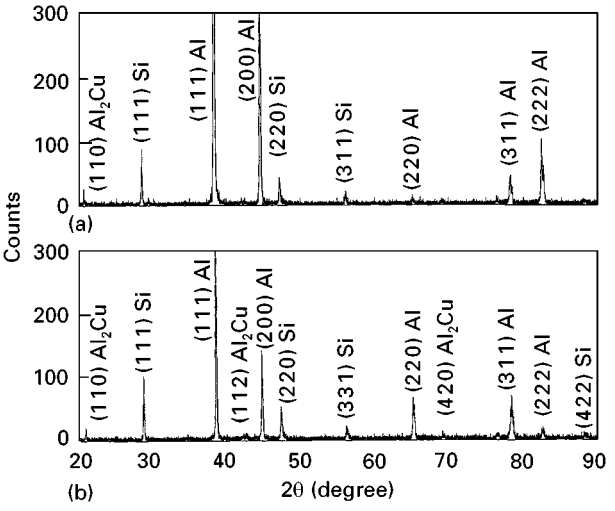

Figure 5 X-ray diffraction patterns of the extruded AS17 alloy in: (a) as-spray deposited condition; (b) as-extruded (extruded at 673 K).

on the concurrent and mutually competitive influences of solidification characteristics of the impinging droplets and ensuing interactions with each other and with the deposition surface.

Since the thickness of the spray deposited material is several orders of magnitude larger than that of a single droplet, the thermal gradients that exist during deposition are very important. The instantaneous average thickness of the spray deposited material (say X) may be readily calculated on the basis of mass balance

$$X = [(J_m/\rho_m A_s)t] \quad (1)$$

where J_m is the mass flow rate, ρ_m is the density of the metal and A_s is the area of the substrate surface. The temperature distribution in the growing deposit can be established from laws of differential thermal energy balance, assuming that heat conduction takes place only in a direction perpendicular to the deposition surface. This appears to be a justifiable assumption considering that both the water-cooled copper substrate and the atomizing gas are the primary sources of heat extraction during deposition.

5.2. Tensile properties

The tensile properties of the spray-processed (AS17) and conventional IM-processed materials are summarized in Table II. Results reveal the spray-processed material (AS17) to have better strength (yield and ultimate tensile) than the conventional IM-processed counterpart at both room and elevated temperatures. The improvement in strength was found to have little influence on ductility quantified in terms of elongation-to-failure and reduction-in-area. Increase in test temperature resulted in a degradation of both yield and ultimate tensile strength for both alloys. For the spray processed alloy the degradation of yield strength was as high as 17% and that of ultimate tensile strength was 16%. However, for the conventional IM-processed alloy an increase in test temperature resulted in a 25% decrease in ambient

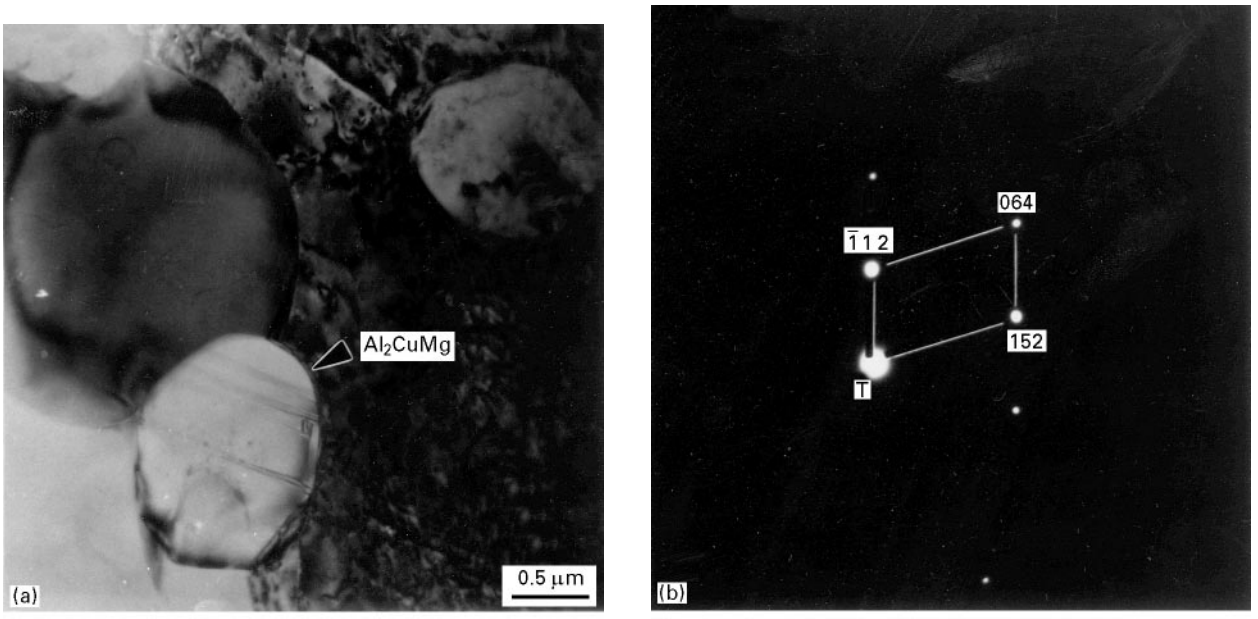

Figure 6 Transmission electron micrograph of AS17 showing the presence of the Al_2CuMg precipitate: (a) Bright-field image; (b) Selected area diffraction, $B = [4\,2\,3]$.

TABLE II Tensile properties of the conventionally processed and spray-processed alloys

Alloy	Processing	Temperature (°C)	Young's modulus[a] (GPa)	Yield strength		Ultimate tensile strength		Elongation (%)	Reduction in area (%)	True strain $\ln(A_o/A_f)$[b] (%)
				MPa	10^3 p.s.i.	MPa	10^3 p.s.i.			
A390	Sand Cast + Extruded	27	78	390	57	424	61	2.4	6.0	7.0
		150	70	283	42	287	42	0.8	2.0	3.0
AS17	Spray-atomized	27	80	411	60	448	65	2.8	6.0	7.0
	and -deposited	150	80	343	50	355	52	2.44	5.0	7.0

[a] Tangency measurement based on extensometer trace.
[b] A_o/A_f is the tensile fracture ductility.

temperature yield strength and a 30% decrease in ultimate tensile strength. The ambient temperature ductility of the spray processed alloy was low and only 2.8% and that of the A390 alloy 2.4%. Increase in test temperature was observed to have a detrimental influence on tensile elongation and reduction-in-area of both alloys. The low ductility of the IM A390 alloy is ascribed to microstructural heterogeneity and is discussed in the following section. A comparison of the engineering stress–engineering strain curves, at the two test temperatures, for the spray deposition-processed and IM-processed A390 alloy, is made in Figs 7 and 8.

Influence of temperature on strain hardening characteristics of the two alloys was evaluated from examining the variation of monotonic stress with plastic strain, plotted on a bilogarithmic scale (Fig. 9). The variation of monotonic stress with plastic strain obeyed the Ramberg–Osgood relationship

$$\varepsilon = \sigma/E + [\sigma/H]^{1/n} \quad (2)$$

where E is the elastic modulus, σ is the stress, n is the strain hardening exponent and H is the monotonic strength coefficient. For each alloy the strain hardening exponent and strength coefficient decreases with an increase in test temperature.

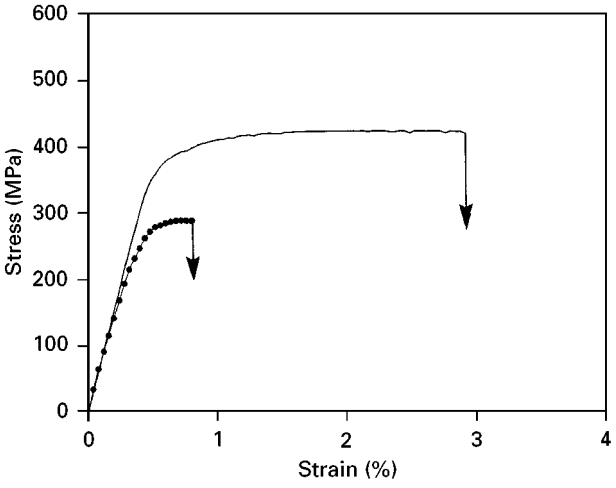

Figure 7 Engineering stress–strain curves for the conventionally processed A390 alloy. (——) 30 °C; (—●—) 150 °C.

Several mechanisms, either independently or in synergism, are considered responsible for the improved strength of the spray-processed material (AS17). The plausible mechanisms include:

1. An overall strengthening resulting from strength of the individual constituents of the alloy, the fine

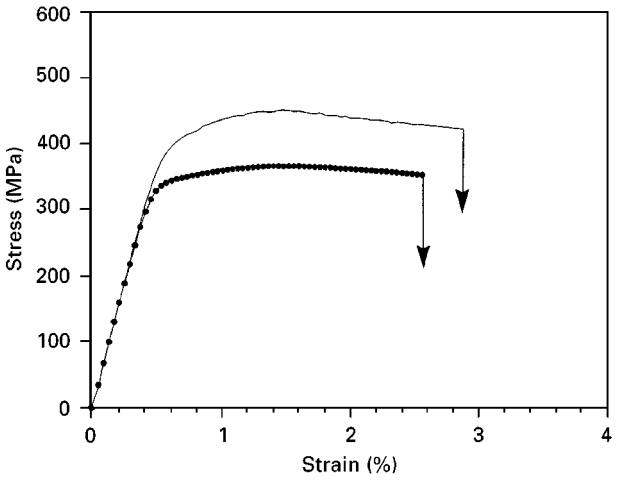

Figure 8 Engineering stress–strain curves for the spray-processed alloy AS17. (——) 30 °C; (—●—) 150 °C.

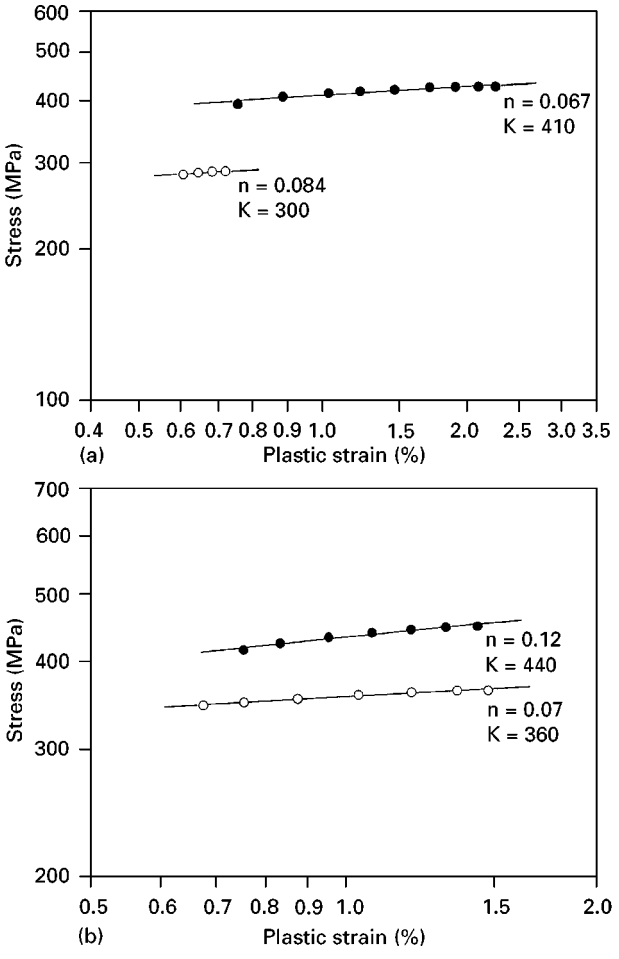

Figure 9 Influence of temperature on monotonic stress–strain response: (a) Conventionally processed; (b) spray processed. (●) 30 °C; (○) 150 °C.

primary particulates of silicon and the alloy matrix, as per the classical rule-of-mixtures (ROM) theory [41].

2. Classical composite strengthening through load transfer from the soft and plastically deforming aluminium alloy matrix to the hard and elastically deforming silicon particulates. The stress and strain transfer is dependent to a large extent on the bond integrity at the particulate–matrix interfaces.

3. Classical Hall–Petch strengthening through contributions from decreased grain size.

4. Residual stresses developed in the alloy matrix and the concomitant plastic strains developed adjacent to the silicon particulates as a direct result of the mismatch in thermal expansion coefficients (ΔCTE) between the constituents of the alloy. The plastic strains are highly localized resulting in a high density of dislocations adjacent to the silicon particulates. The higher dislocation density tends to locally work harden the matrix and thus modify the plastic response.

5. Contributions from texture arising from intrinsic differences in microstructure between the spray deposition processed and the conventional ingot metallurgy processed counterpart.

The hypereutectic aluminium–silicon alloy used in this study can be considered as being equivalent to a metal–matrix composite (MMC) with a soft and plastically deforming aluminium alloy matrix interdispersed with hard and elastically deforming silicon particulates. A well-defined microstructural characteristic of aluminium alloy-based MMCs that are discontinuously reinforced with fine ceramic particulate or whisker reinforcements is the presence of a high density of immobile dislocations. Independent studies have found the dislocation density in aluminium alloy-based MMCs to be as high as 10^{13}–$10^{14}\,m^{-2}$ in the immediate vicinity of particulate–matrix interfaces [43, 44]. The generation of these immobile dislocations was attributed to the large difference in thermal expansion coefficients (ΔCTE) between the ceramic reinforcements and the metal matrices [43, 44]. The ΔCTE generated high dislocation density between the constituents of the composite is a major contribution to strengthening of the discontinuously-reinforced aluminium alloy-based MMCs [45]. A comparison of the CTEs of aluminium, silicon carbide and pure silicon indicates that the CTEs of aluminium and SiC are $23.2 \times 10^{-6}\,K^{-1}$ and $4.6 \times 10^{-6}\,K^{-1}$, an order of six difference, respectively, whereas that of pure silicon is $2.5 \times 10^{-6}\,K^{-1}$ (an order of ten). Since the difference in CTE between aluminium and pure silicon is greater than that between aluminium and SiC (an order of six), a higher dislocation density due to ΔCTE is expected in the former combination. Therefore, considering the large difference in the thermal expansion coefficients of aluminium and silicon, contributions to strengthening by the immobile dislocations cannot be ignored.

The plausible mechanisms contributing significantly to the improved strength of the spray atomized and deposited alloy are the concurrent and mutually interactive influences of (a) classical composite strengthening, (b) presence of immobile dislocations, and (c) grain size effect. On the basis of classical dislocation strengthening theory the increment in strength due to an increase in dislocation density can be expressed as

$$\Delta\sigma = \alpha G b (\Delta\rho)^{1/2} \quad (3)$$

where α is the constant (1.25), G is the shear modulus of aluminium (28 GPa), and b is the Burger's vector

(0.283 nm). The large difference in CTE results in misfit or mismatch strains at the matrix–silicon particulate interfaces.

5.3. Tensile deformation and fracture

The tensile fracture surfaces are helpful in elucidating processing and microstructural influences, on strength, ductility and fracture-related properties of the hypereutectic alloy. Representative fracture features of the two alloys are shown in Figs 10–14. The fracture behavior of each alloy, at the two test temperatures, is discussed separately.

5.3.1. Spray-processed alloy

At both ambient (27 °C) (Fig. 10) and elevated (150 °C) (Fig. 11) temperatures fracture of this alloy exhibited macroscopically brittle failure with the fracture occurring on a plane normal to the far-field stress axis. However, at the microscopic level the fracture surface revealed features reminiscent of locally ductile failure. High magnification observations revealed a population of voids of varying size, isolated pockets of shallow dimples and fine microscopic cracks. The existence of fine microscopic voids provides convincing evidence as to their formation and presence from spray-deposition processing. The fine microscopic cracks were dispersed in the centre of the dimples and along the grain boundaries. The macroscopically brittle, macroscopically ductile failure mode accords well with that of aluminium alloy-based matrices reinforced with fine ceramic particulates. The average size of the dimple was larger than the average size of the silicon particulates indicative of the extensive plasticity sustaining capability of this microstructure at the microscopic level.

At the elevated temperature the fracture surface (Fig. 11) revealed numerous macroscopic voids inter-

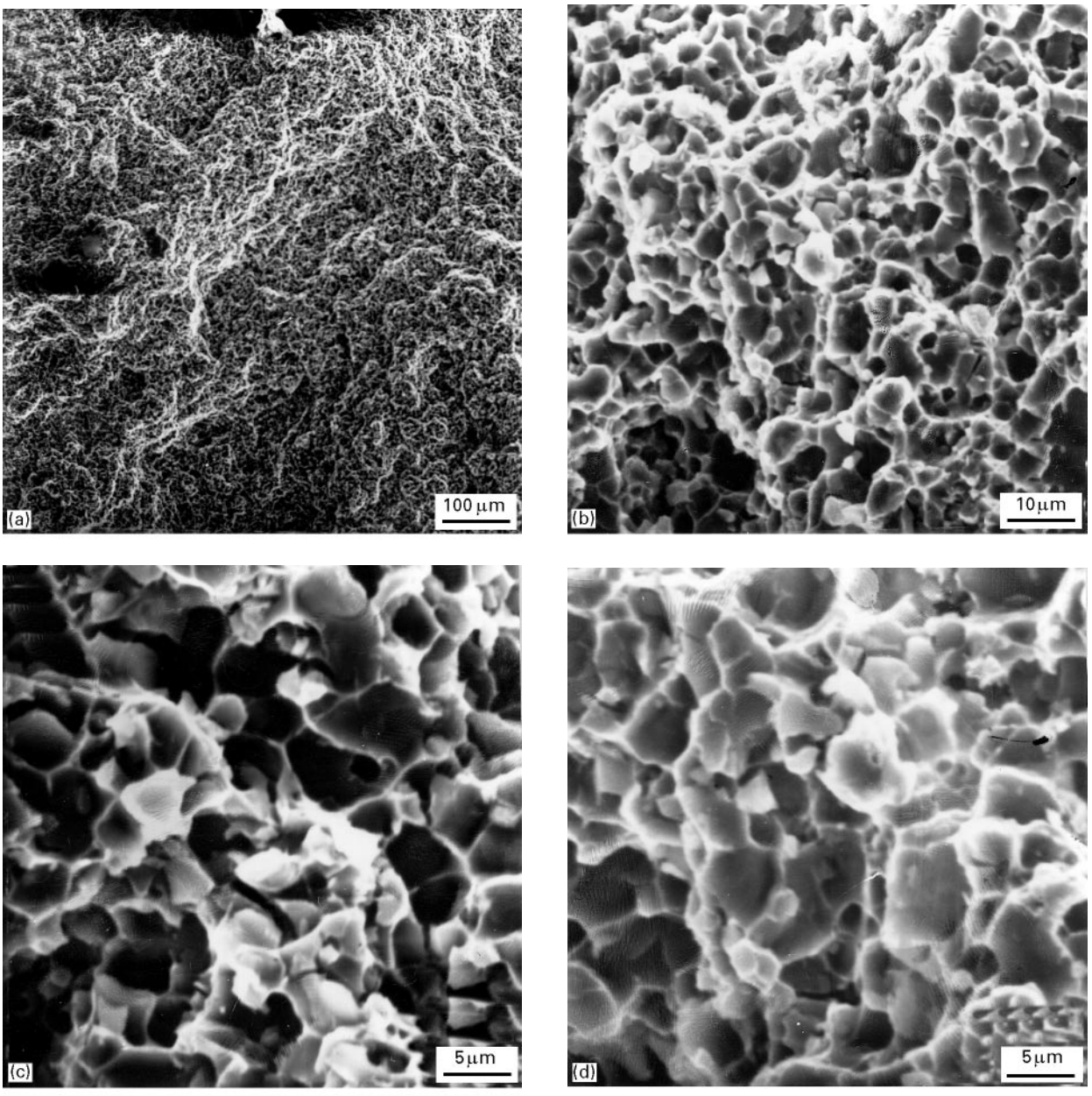

Figure 10 Scanning electron micrographs of the tensile fracture surface of the spray processed alloy deformed at ambient temperature (30 °C).

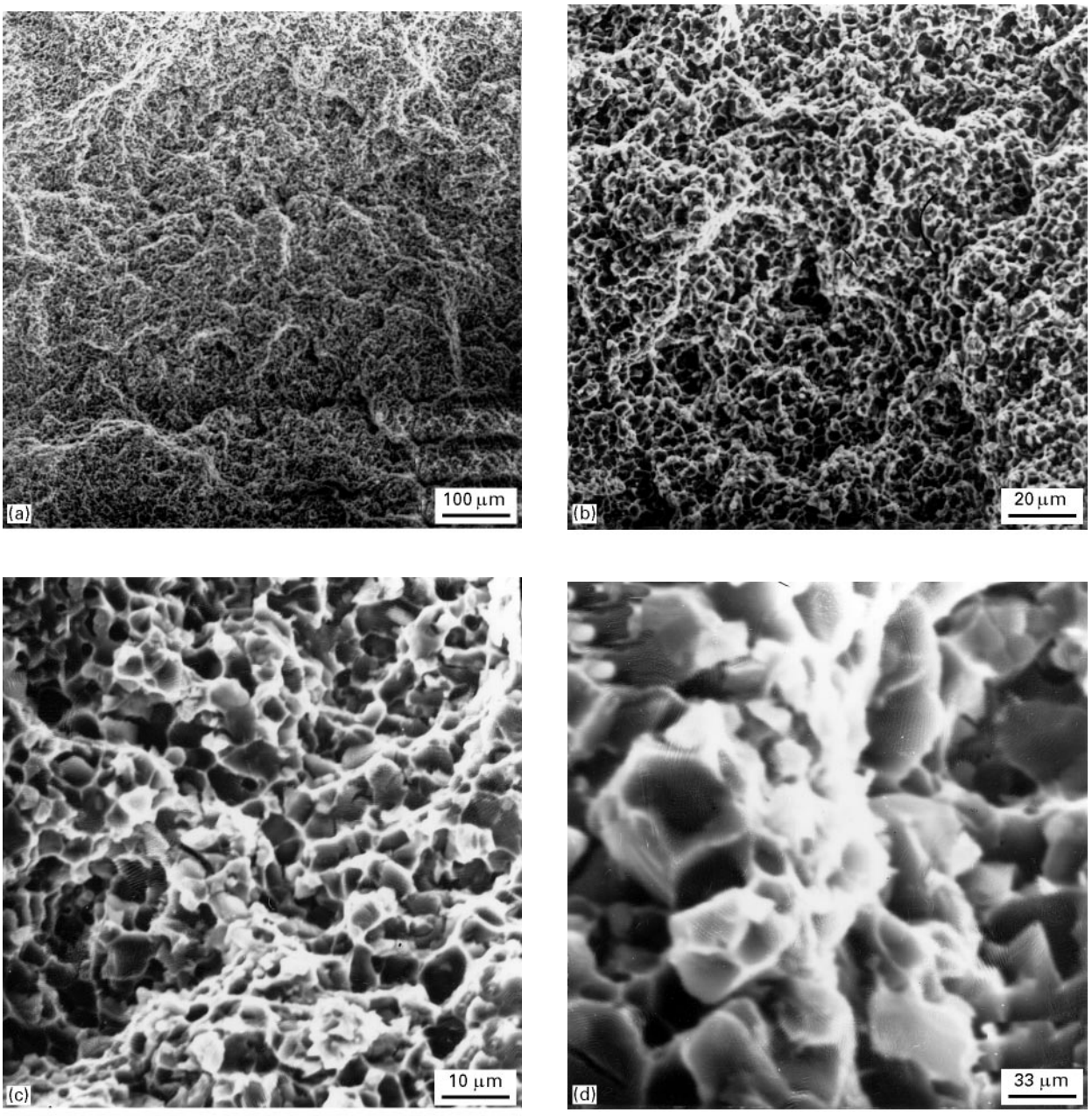

Figure 11 Scanning electron micrographs of the tensile fracture surface of the spray processed alloy deformed at elevated temperature (150 °C).

mingled with fine microscopic voids and shallow dimples, features reminiscent of locally ductile failure. Microscopic fracture features were identical to that observed at the lower test temperature. Isolated pockets of microscopic cracks were found in the central region of the dimples. The suppression of grain boundary fracture in this microstructure results in the intervention of the higher energy absorbing fracture mode, that is, ductile transgranular rupture. However, the macroscopic fracture surface appearance of this alloy does not correlate well with observed macroscopic ductility, primarily because final fracture is a combination of voids, ductile dimples and microscopic cracking. The overall number density and size of the dimples did reveal significant difference in microplasticity between the spray processed and conventional ingot processed counterpart.

5.3.2. Ingot cast and extruded

At both room (27 °C) and elevated (150 °C) temperatures fracture of this alloy exhibited macroscopically brittle failure with fracture occurring essentially normal to the tensile stress axis. On a microscopic scale, the surface morphology was rough (Fig. 12a) and covered with numerous pockets of macroscopic and fine microscopic voids (Fig. 12b). High magnification examination of the tensile fracture surface revealed features reminiscent of locally ductile and brittle mechanisms through the presence of a population of dimples of varying size, numerous fine microscopic cracks (Fig. 12c) and cracked particulates of coarse primary silicon (Fig. 12d).

The test specimen deformed to failure at the elevated temperature revealed, at the microscopic level, the fracture surface to be covered with: (i) numerous

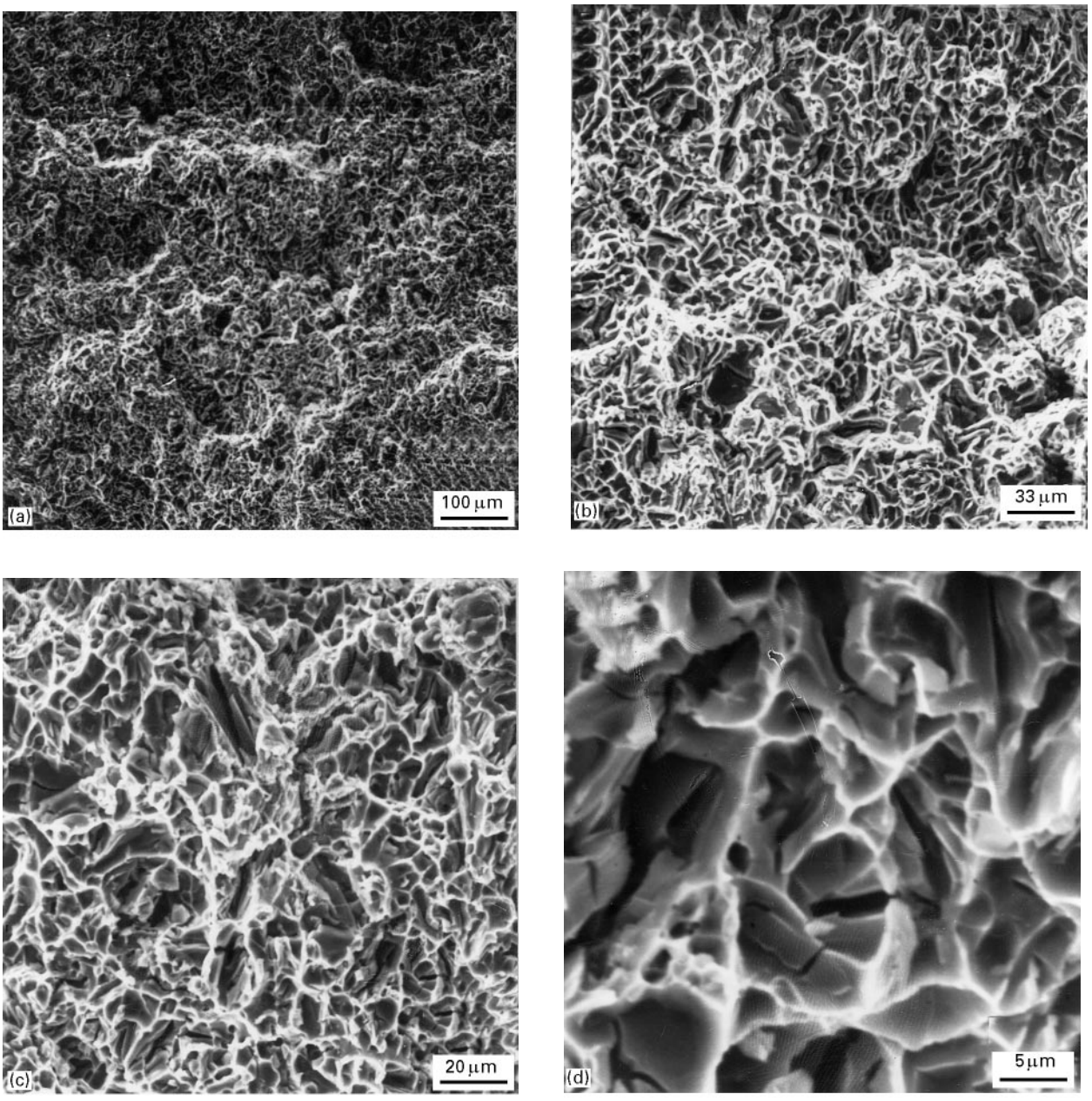

Figure 12 Scanning electron micrographs of the tensile fracture surface of the conventionally processed alloy deformed at ambient temperature (30 °C).

macroscopic voids (Fig. 13a), (ii) cracked particulates of coarse primary silicon (Fig. 13b), (iii) numerous fine microscopic cracks, and (iv) isolated pockets of shallow dimples (Fig. 13c). The macroscopic and fine microscopic voids were intermingled with tear ridges and isolated regions of dimpled rupture (Fig. 13d). The presence of numerous macroscopic voids coupled with fine microscopic voids, of varying size, is largely responsible for the degradation in strength and the inferior ductility at this temperature. Multiple microscopic cracks were observed in regions adjacent to the silicon particulate which contributed to the observed degradation in tensile ductility. Examination of the fracture surfaces at high magnification revealed the damage to be highly localized at the coarse primary silicon through cracked particulates and interfacial failure or decohesion. This suggests the plastic strain becomes localized during the early stages of tensile deformation. The intrinsic brittleness of the silicon particulates coupled with the propensity for it to fracture due to localized deformation resulted in particle cracking and interface failure through debonding being the dominant damage modes. Furthermore, the triaxial stresses generated, at the microscopic level, during far-field tensile loading favours limited growth of the fine microscopic voids in the matrix. Very few of the fine microscopic voids grow and coalesce and the halves of these voids are the isolated pockets of shallow dimples observed on the tensile fracture surface. The fracture plane of the cracked silicon particulates was essentially perpendicular to the loading axis (Fig. 14) suggesting the importance of the tensile stress in inducing particulate fracture. A careful examination of the tensile fracture surface of this alloy revealed that in excess of 50% of the silicon particulates had fractured during tensile deformation.

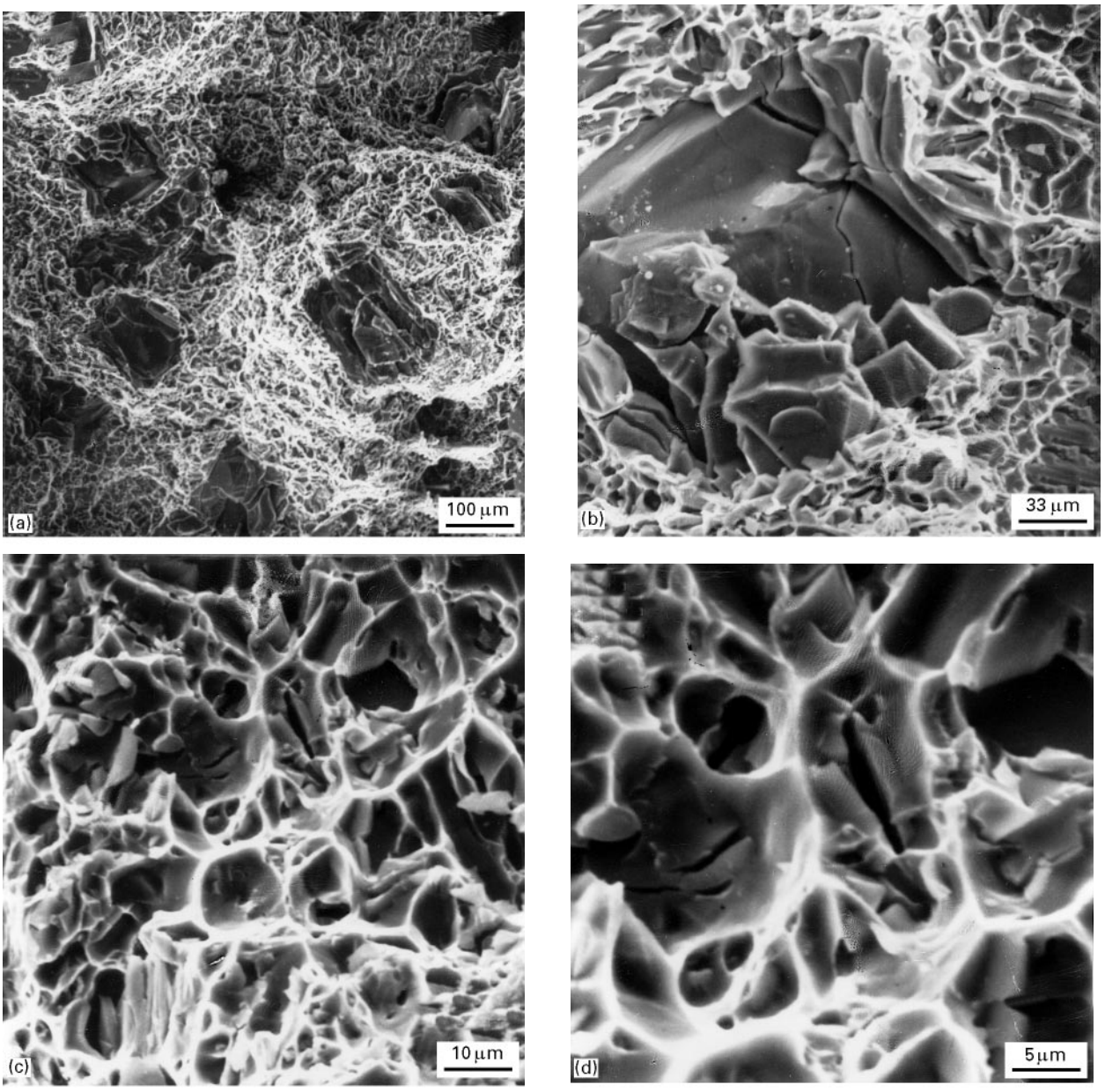

Figure 13 Scanning electron micrographs of the tensile fracture surface of the conventionally processed alloy deformed at elevated temperature (150 °C).

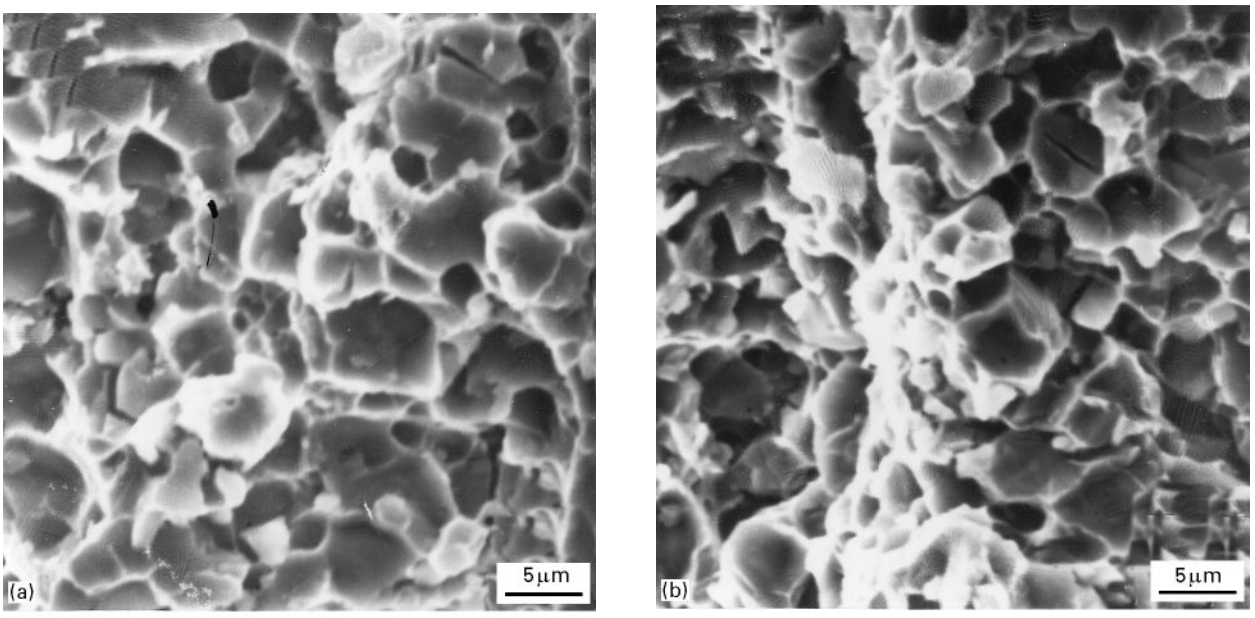

Figure 14 Scanning electron micrograph showing cracked particulates normal to the far-field stress axis.

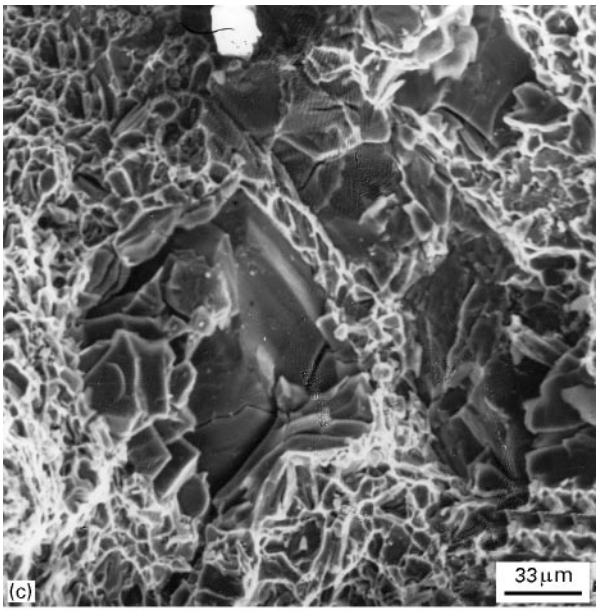

Figure 14 (continued).

This indicates that not all of the particles were loaded to their fracture stress suggesting the non-uniform size and distribution of the particulates in the alloy matrix. Assuming that damage initiates early in the conventionally processed alloy due to localized stresses and strain, the matrix microstructure plays an important role in governing flow localization and damage coalescence.

6. Conclusions

A study of the microstructure and resultant fracture behaviour of spray atomized and deposited hypereutectic aluminium-silicon alloy provides the following conclusions:

1. Microstructure of a conventional ingot metallurgy processed alloy revealed coarse silicon particulates, of varying size, distributed randomly through the microstructure. At regular intervals the particulates revealed agglomeration. The spray-atomized and deposited alloy revealed fine particulate shaped silicon dispersoids distributed uniformly through the microstructure and equiaxed shaped grains.

2. Tensile properties of the spray-processed alloy (AS17) is superior to the conventional IM (A390-T6) counterpart. Increase in temperature caused a degradation of both yield and ultimate tensile strength. Factors contributing to the improved strength of the spray-processed alloy are discussed in light of processing influences, differences in thermal expansion coefficient, and contributions from constituents based on the theory of composite mechanics.

3. Tensile fracture of the spray atomized and deposited alloy (AS17), at the microscopic level, was predominantly transgranular with little evidence of intergranular failure and particulate cracking. Suppression of microcracking either through particulate failure or grain boundary failure resulted in enhanced microplasticity and a higher energy absorbing transgranular fracture mode. Macroscopic and microscopic voids and shallow dimples were evident on the fracture surface, features reminiscent of locally ductile failure.

Acknowledgements

This research was supported by National Aeronautics and Space Administration: Langley VA (Grant no. NAGI-1619) and partially by The University of Akron (Grant no. 2-0799) with material support from Reynolds Metals Company (Richmond, VA).

References

1. F. YILMAZ and R. ELLIOTT, *J. Mater. Sci.* **24** (1989) 2065.
2. N. KUROISHI, Y. ODANI and Y. TAKEDA, *Met. Powd. Rep.* **40** (1985) 642.
3. J. ZHOU, J. DUSZCZYK and B. M. KOROVAAR, *J. Mater. Sci.* **26** (1991) 3041.
4. I. YAMAGUCHI, I. OHNAKA, S. KAWAMOTO and T. FUKUSAKO, *Trans. Japan Inst. Met.* **27** (1986) 196.
5. M. MOTOMURA, T. HAGA and Y. SAKURAI, *J. Japan Inst. Light Metals* **38** (1988) 528.
6. J. J. ESTRADA and J. DUSZCZYK, *J. Mater. Sci.* **25** (1990) 1381.
7. J. ZHOU and J. DUSZCZYK, *ibid.* **25** (1990) 4541.
8. N. HANDIAK, J. E. GRUZLESKI and D. ARGO, *Trans. Amer. Foundrymen Soc.* **95** (1987) 31.
9. Y. B. SUN and C. R. LOPER, Jr, in Proceedings of the Second International Conference on Molten Aluminium Processing, Orlando, FL, (American Foundrymen Society, Chicago, 1989) p. 71.
10. A. R. E. SINGER, *Met. Powd. Rep.* **41** (1986) 117.
11. E. J. LAVERNIA, *Int. J. Rapid Solidification* **5** (1989) 47.
12. P. MATHUR and A. LAWLEY, *J. Metals* **41** (1989) 23.
13. M. GUPTA, E. J. LAVERNIA and F. A. MOHAMED, *Mater. Manuf. Proc.* **5** (1990) 165.
14. E. J. LAVERNIA, J. D. AYERS and T. S. SRIVASTAN, *Int. Mater. Rev.* **37** (1992) 1.
15. M. GUPTA, F. A. MOHAMED and E. J. LAVERNIA, *Metall. Trans.* **23A** (1992) 831.
16. X. LIANG and E. J. LAVERNIA, *Mater. Sci. Engng* (1995) **148** (1995) 100.
17. YUE. WU and E. J. LAVERNIA, *J. Metals* **43** (1991) 32.
18. M. GUPTA, F. A. MOHAMED and E. J. LAVERNIA, *Mater. Sci. Engng* **144A** (1991) 99.
19. T. S. SRIVATSAN, T. S. SUDARSHAN and E. J. LAVERNIA, *Progr. Mater. Sci.* **39** (1995) 317.
20. R. MEHRABIAN, *Int. Metals Rev.* **24** (1982) 186.
21. P. MATHUR, D. APELIAN and A. LAWLEY, *Acta Metall.* **37** (1989) 429.
22. E. M. GUTIERREZ, E. J. LAVERNIA, G. M. TRAPAGA, J. SZEKELY and N. J. GRANT, *Metall. Trans.* **20A** (1989) 71.
23. M. GUPTA, F. A. MOHAMED and E. J. LAVERNIA, *Int. J. Rapid Solidification* **6** (1991) 247.
24. X. LIANG and E. J. LAVERNIA, *Mater. Sci. Engng* **153A** (1992) 646.
25. X. LIANG, J. EARTHMAN and E. J. LAVERNIA, *Acta Metall.* **40** (1992) 3003.
26. E. J. LAVERNIA, T. S. SRIVATSAN, R. H. RANGEL, *Atomization and Sprays* **2** (1992) 253–274.
27. X. LIANG, H. K. KIM, J. C. EARTHMAN and E. J. LAVERNIA, *Mater. Sci. Engng* **153A** (1992) 646.
28. M. GUPTA, T. S. SRIVATSAN, A. MOHAMED and E. J. LAVERNIA, *J. Mater. Sci.* **28** (1993) 2245.
29. S. PING YAN, F. A. MOHAMED, T. S. SRIVATSAN and E. J. LAVERNIA, *ibid.* **30** (1995) 4726.
30. J. ZHANG, M. N. GUNGOR and E. J. LAVERNIA, *ibid.* **28** (1993) 1515.

31. YUE WU, W. A. CASSADA and E. J. LAVERNIA, *Metall. Trans.* **26A** (1995) 1235.
32. D. C. JENKINSON and L. M. HOGAN, *J. Cryst. Growth* **28** (1975) 171.
33. S. N. OHJA, J. N. JHA and S. N. SINGH, *Scripta Metall. Mater.* **25** (1991) 443.
34. S. ANNAVARAPU, D. APELIAN and A. LAWLEY, *Metall. Trans.* **21A** (1990) 3237.
35. J. ZHOU and J. DUSZCZYK, in Proceedings of the First European Conference on Advanced Materials and Processes, Aachen, Germany, 1990, edited by H. E. Exner and V. Schaumacher, vol. 1, p. 241.
36. T. S. SRIVATSAN and E. J. LAVERNIA, *J. Mater. Sci.* **27** (1992) 5965.
37. E. J. LAVERNIA, *Int. J. Rapid Solidification* **5** (1989) 47.
38. E. J. LAVERNIA, E. GUTIERREZ, J. SZAKELY and N. J. GRANT, *Progr. Powd. Metall.* **43** (1987) 683.
39. S. ANNAVARAPU, D. APELIAN and A. LAWLEY, *Metall. Trans.* **19A** (1988) 3077.
40. M. SHAMSUZZOHA and L. M. HOGAN, *J. Cryst. Growth* **76** (1986) 429.
41. C. J. DVORAK, in "Metall matrix composites: mechanisms and properties", edited by R. K. Everett and R. J. Arsenault (Academic Press, San Diego, CA, 1991) p. 1.
42. V. C. NARDONE, *Scripta Metall.* **21** (1987) 1313.
43. M. VOGELSANG, R. J. ARSENAULT and R. M. FISHER, *Metall. Trans.* **127A** (1986) 379.
44. R. J. ARSENAULT and N. SHI, *Mater. Sci. Engng* **A81** (1986) 175.
45. R. J. ARSENAULT, *Scripta Metall. Mater.* **25** (1991) 2617.
46. F. K. N. NABARRO, Z. S. BASINSKI and D. B. HOLT, *Adv. Phys.* **13** (1964) 193.
47. T. S. SRIVATSAN and E. J. LAVERNIA, in "Processing and fabrication of advanced materials for high temperature applications II, edited by V. A. Ravi and T. S. Srivatsan, (The Minerals, Metals and Materials Society, Warrendale, PA, 1993) p. 141.

Received 27 August
and accepted 23 October 1996